Hindawi
Mathematical Problems in Engineering
Volume 2022, Article ID 6978943, 12 pages
https://doi.org/10.1155/2022/6978943

Research Article

Pushing Pose Sensing of Underground Mobile Supporting Robot

Nan Wang,[1] Hao Liu,[1] Xiaobiao Li,[1] Meizi Tian,[2] and Lin Zhang [2,3]

[1]*School of Mechanical and Electronic Engineering, Suzhou University, Suzhou 234000, China*
[2]*School of Robot Engineering, Yangtze Normal University, Chongqing 408100, China*
[3]*School of Mechanical Engineering, Shanghai Jiao Tong University, Shanghai 200240, China*

Correspondence should be addressed to Lin Zhang; lin.zhang_2014@hotmail.com

Received 23 March 2022; Revised 15 April 2022; Accepted 22 April 2022; Published 8 June 2022

Academic Editor: Jorge Cunha

The pushing pose of underground mobile supporting robot (MSR), i.e., hydraulic support, is a key factor to measure the straightness of the working face. Therefore, in order to independently complete the pushing process and ensure the straightness requirements of the pushing pose, by considering the pushing displacement of MSR and the pose of the middle groove of the scraper conveyor, this study proposes a fusion evaluation model combined with the least square straightness based on the pushing displacement and the straightness based on the pose of the middle groove. The pose sensing approach is established by estimating the pose of the middle groove and the displacement of MSR, analyzing, and extracting the data characteristics of acceleration signal; the OVR (one-versus-rest) method is used to realize the displacement state pattern recognition of hydraulic support based on SVM (support vector machine). The effectiveness of this approach is verified by building an experimental platform.

1. Introduction

As an important intelligent equipment for fully mechanized mining, mobile supporting robot (MSR, also known as hydraulic support) uses high-pressure emulsion to realize the cyclic actions and provides support and protection for the fully mechanized mining face [1]. The pushing pose of MSR refers to the pose state formed by the middle groove of the scraper conveyor when MSR pushes forward with the working face, pushed and moved periodically [2]. In the process of coal mining, MSR, scraper conveyor, and coal wall need to maintain a certain straightness to ensure the smooth operation of coal mining equipment [3–6]. However, the pushing pose of MSR is the essential factor for the straightness of the working face. Therefore, in order to ensure the good straightness of the working face, it is necessary to study the sensing approach of the pushing pose of MSR and realize the straightness evaluation of the pose of MSR.

At present, the pose sensing approach of MSR mainly depends on the displacement sensor installed in MSR pushing jack. However, approach has large systematic error. At the same time, it is complicated to replace the damaged sensors because of the poor working conditions and heavy equipment. Thus, it is very necessary to study a new approach to sense MSR pose. Based on the sensing of MSR pose and considering the influencing factors of the change of the middle groove pose, this study established the pushing pose straightness evaluation model based on the pushing displacement and the middle groove pose of the scraper conveyor, which provided the model basis and constraint target for the independent pushing of MSR.

2. Related Work

At present, the sensing approach for pose and straightness of hydraulic support mainly focus on simple on-site pull wire and infrared beam measurement. With the deep integration of intelligent detection technology into coal mine production, the inertial navigation technology [6, 7], Unity3D technology [8–11], and visual technology [12, 13] have been used gradually. Zhang et al. and Chen et al. [3, 14] proposed a pose monitoring method of hydraulic support based on multisensor fusion technology. Yang et al. [15] and Liang et al. [16] used the lidar and inclination sensors to measure the pose of hydraulic support, respectively. Wang et al. [17]

proposed a method for measuring the height and straightness of the hydraulic support group based on point cloud; analyzing the geometric posture of single hydraulic support point cloud, the feature points are selected on each hydraulic support to solve the straightness, which effectively reduce the matching error. Wang et al. [18] realized the continuously adjusted for alignment without the interrupt of longwall face based on the reference target line with absolute direction. In addition, multisoftware cosimulation [19], information fusion [20, 21], and algorithm fusion [22, 23] are used in straightness detection of hydraulic support.

Although the above approaches have been verified by theory and experiment, the environment in the coal mine has lots of dust and the oil circuit on the hydraulic support is complex, resulting in the obstruction of sight and the limited use of indirect measurement technology. Meanwhile, the existing position sensor is installed inside the hydraulic jack with high error. In order to solve these problems, in this study, the IMU (inertial measurement unit) installed on the middle groove of scraper conveyor is used to directly measure the displacement acceleration, and the MS-KF (multisegmental Kalman filter) approach is used to eliminate the accumulation error. By considering the sensing of the hydraulic support pose and the change of middle groove pose, established the pushing pose straightness evaluation model combined the pushing displacement and the middle groove pose, which provided the model basis and constraint target for the independent pushing of the hydraulic support.

3. Pose Sensing Based on Pushing State Recognition

At present, the sensors used by the electrohydraulic control system of MSR in collecting the displacement information are built in the push jack, but this method has sensing error and unfavorable for the installation and maintenance of the sensor. In order to solve these problems, IMU installed on the middle groove of the scraper conveyor is used to directly measure the displacement. However, there is a large time accumulation error in the method of using IMU to collect the acceleration in the process of moving and calculating the pushing displacement through integral processing. Therefore, it is necessary to study more effective error elimination methods to realize the accurate measurement of pushing pose based on IMU.

In the pushing process of MSR, the jack will quickly enter the uniform motion state from the static state, which is called the instantaneous acceleration state. After a period of time, it will quickly enter the static state from the uniform state, which is called the instantaneous deceleration state. The instantaneous acceleration and instantaneous deceleration state are called variable velocity state (VVS). Uniform motion state is called constant velocity state (CVS). Other stages remain at static state which is called zero velocity state (ZVS).

According to the above prior knowledge, the acceleration data in different states are processed in sections: the Kalman filtering method of the variable acceleration model be used in VVS, the Kalman filtering method of the zero acceleration model be used in CVS, and ZVS provides the reference point of zero velocity update for the whole process of displacement estimation. Compared with the traditional method, it does not use all the data for Kalman filtering calculation, but only uses the data in VVS and CVS periods, so it can reduce the source of cumulative error. In addition, a priori knowledge about velocity and acceleration is added in VVS and CVS periods; the Kalman state space conversion model in the two periods is refined, finally reducing the measurement error.

3.1. Methods. This method recognizes the pushing state with the acceleration signal collected; different Kalman filter state space conversion models are applied in different states; meanwhile, the reference point of ZUPT is provided in the ZVS period, which will reduce the measurement error. In essence, the method is called the multiphased Kalman filter (MS-KF) because of subsection handling a group of acceleration time series with the Kalman filter. The method architecture is shown in Figure 1, and the key technical process is as follows.

3.1.1. Estimation of Middle Groove Pose. The acceleration signal collected by IMU is affected by gravity. In order to remove the influence caused by gravity, we need to obtain the direction of gravity component through pose estimation with the help of gyroscope information output by IMU and then remove the acceleration component caused by gravity. The pose of the middle groove can be estimated by the following formula:

$$\begin{aligned} {}^{L}_{G}q_{w,t} &= \frac{1}{2}{}^{L}_{G}q_{t-1} \otimes {}^{L}\omega_{t}, \\ {}^{L}_{G}q_{w,t} &= {}^{L}_{G}q_{w,t-1} + {}^{L}_{G}q_{w,t}\Delta t, \end{aligned} \tag{1}$$

where ${}^{L}\omega_{t}$ is the angular rate relative to the sensing coordinate system at time t, ${}^{L}_{G}q_{t-1}$ is the rotation quaternion of the world coordinate system relative to the sensing coordinate system at time $t-1$, and ${}^{L}_{G}q_{w,t}$ is the rotation quaternion of the world coordinate system relative to the sensing coordinate system at t-time.

Through the following formula, the acceleration signal in the sensing coordinate system can be converted into the acceleration signal in the world coordinate system.

$${}^{G}g' = R\left({}^{L}_{G}q_{w,t}\right){}^{L}\alpha_{t}. \tag{2}$$

Among them, $R(\cdot)$ converts the pose represented by quaternion into matrix form, and the conversion formula is

$$R(q) = \begin{bmatrix} q_0^2 + q_1^2 - q_2^2 - q_3^2 & 2(q_1q_2 - q_0q_3) & 2(q_1q_3 + q_0q_2) \\ 2(q_1q_2 + q_0q_3) & q_0^2 - q_1^2 + q_2^2 - q_3^2 & 2(q_2q_3 - q_0q_1) \\ 2(q_1q_3 - q_0q_2) & 2(q_3q_2 + q_0q_1) & q_0^2 - q_1^2 - q_2^2 + q_3^2 \end{bmatrix}. \tag{3}$$

Theoretically, the acceleration signal caused by gravity meets the following equation after conversion:

$$R\left(\Delta q_{acc}\right){}^{G}g_{r} = {}^{G}g', \tag{4}$$

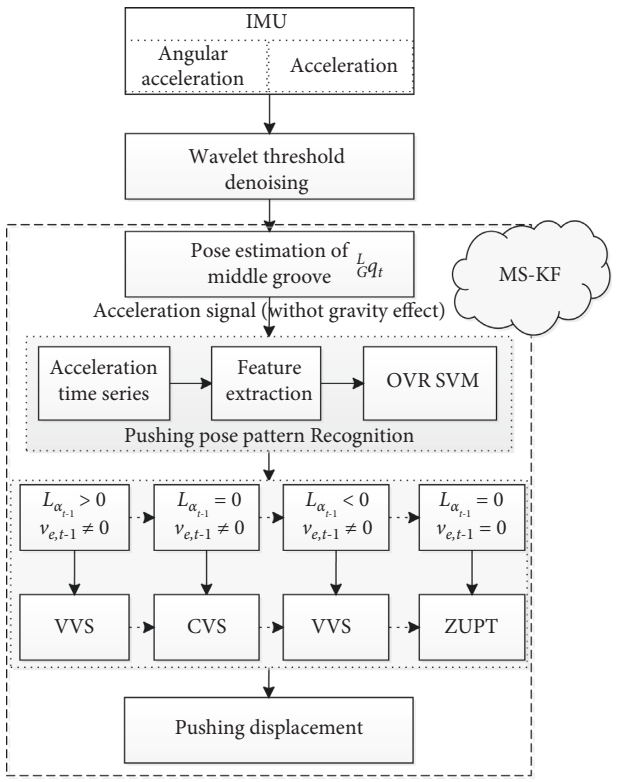

Figure 1: Pushing displacement sensing architecture.

where ${}^{G}g_r$ is the true gravity vector, the theoretical value is ${}^{G}g_r = [0, 0, g]^T$. In practice, deviation $\Delta\widehat{q}_{acc}$ may exist. The final pose can be obtained by quaternion interpolation through SLERP and other methods:

$$ {}^{L}_{G}q_t = {}^{L}_{G}q_w \otimes \Delta\widehat{q}_{acc}. \tag{5} $$

Through the above steps, it not only can calculate the pose of the middle groove but also can pretreat the acceleration signal, removing the component generated by gravity in the acceleration signal.

3.1.2. Displacement Estimation Based on MS-KF. After the pose estimation of the middle groove, the collected acceleration signals are transformed into the acceleration time series without the influence of gravity, the data characteristics of the acceleration signals are analyzed and extracted, and the SVM is used for training. Finally, the displacement state of the acceleration time series can be recognized by using the trained SVM model.

For acceleration time series under different transition states, MS-KF will use different state space models to estimate the transition displacement. Delimiting the displacement and velocity variables x_t and v_t , respectively, the state space model of VVS section is

$$ \begin{bmatrix} x_{e,t} \\ v_{e,t} \\ {}^{L}a_{e,t} \end{bmatrix} = \begin{bmatrix} I & \Delta tI & I\Delta t^2/2 \\ 0 & I & R({}^{L}_{G}q_t)\Delta t \\ 0 & 0 & I \end{bmatrix} \begin{bmatrix} x_{e,t-1} \\ v_{e,t-1} \\ {}^{L}a_{e,t-1} \end{bmatrix} + \begin{bmatrix} 0 \\ -g\Delta t \\ 0 \end{bmatrix} + v_t. \tag{6} $$

Among them, v_t refers to the processing noise. For the acceleration in the CVS period, theoretically, the acceleration should be 0, so the state space model adopted by CVS is

$$ \begin{bmatrix} x_{i,t+1} \\ v_{i,t+1} \\ {}^{L}a_{i,t+1} \end{bmatrix} = \begin{bmatrix} I & \Delta tI & 1/2I\Delta t^2 \\ 0 & I & R({}^{L}_{G}q_t)\Delta t \\ 0 & 0 & 0 \end{bmatrix} \begin{bmatrix} x_{i,t} \\ v_{i,t} \\ {}^{L}a_{i,t} \end{bmatrix} + \begin{bmatrix} 0 \\ -g\Delta t \\ 0 \end{bmatrix} + v_t. \tag{7} $$

Second, different initial state values need to be set for acceleration time series in different phases when Kalman filtering estimation is carried out. The initial value setting is shown in the following formula:

$$ X_t = \begin{cases} X_{e,t} | \{X_{e,0} = 0, P_0 = 0\}, \text{mean}(\{x_i\}) > 0, & x_i \in VVS, \\ X_{i,t}, & y_i \in CVS, \\ X_{e,t} | \{X_{e,0} = X_{i,t}, P_0 = 0\}, \text{mean}(\{x_i\}) < 0, & x_i \in VVS. \end{cases} \tag{8} $$

Among them, X_t is the state variable, $X_t = [x_{i,t}, v_{i,t}, {}^{L}a_{i,t}]^T$, and $X_{e,0}$ and P_0 are the initial values of state variables and estimation errors in Kalman filter estimation, respectively. MS-KF can be realized with the above steps.

3.2. Feature Extraction and Selection. Before realizing MS-KF, it is necessary to subsection the process of acceleration time series. In order to study the data characteristics of acceleration time series in the process of MSR pushing, the pushing displacement signal and acceleration signal collected in the laboratory environment are collected, as shown in Figures 2(a) and 2(b), respectively, finally getting the schematic diagram of their characteristics with denoising and normalizing the signal, as shown in Figure 2(c). At the beginning of sliding, the positive component of acceleration is large and reaches the average speed of moving jack in a very short time. At the end of sliding, there is a small acceleration change. After the above actions, a sliding process is completed. It is the opposite when moving the support; first, at the beginning of support-moving, the negative component of acceleration is large and then moving at a uniform speed after reaching the average speed of support-moving. At the end of the support-moving, there is a small change, and then, it enters the static state.

MS-KF analysis is based on recognizing the acceleration in VVS, ZVS, and CVS periods. However, when jack is working in the VVS area, the time of accelerating and decelerating is very short, the feature discrimination corresponding to each state is low, and the final recognition effect will be affected. Therefore, it cannot improve the recognition rate through recognizing the state of acceleration signal directly. According to the above analysis of the pushing process, MSR corresponds to the four states of sliding start (S1), pushing end (S2), support-moving start (S3), and support-moving end (S4) in a pushing cycle. VVS corresponds to the area that state transition from one to another. CVS corresponds to the area not only between S1 and S2 but also between S3 and S4. ZVS corresponds to other areas. This method uses the prior knowledge of the transition system in state pattern recognition, which is more efficient and reliable, and the accuracy of final recognition will be improved.

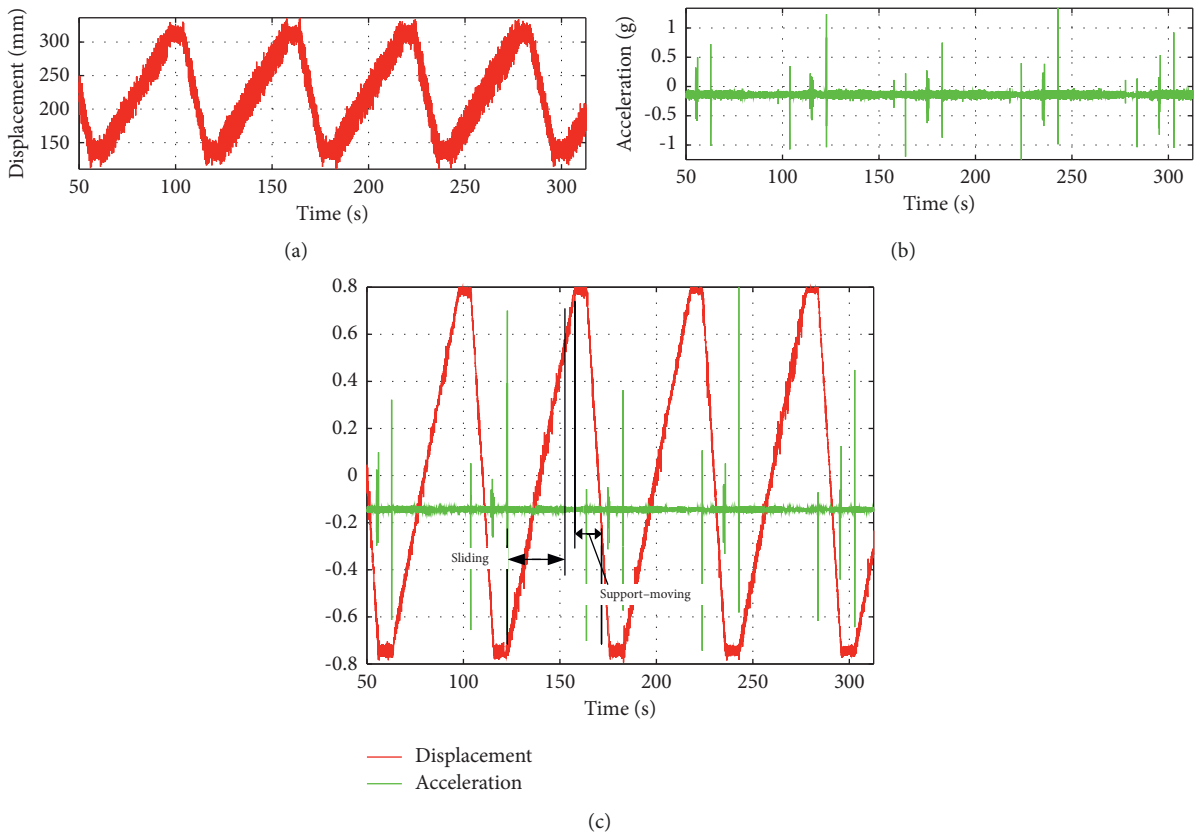

Figure 2: Feature samples of acceleration and displacement.

Extracting and selecting effective data features is the premise of pushing state pattern recognition. For the acceleration signal, the features that can be extracted are as follows:

(1) Average power: describing the vibration intensity of the signal, $x(n)$ is the collected acceleration time series, where n is the length of the time series, $n = 1, 2, 3...N$. The characteristic value can be calculated according to the following formula:

$$f_1 = \sum_{n=1}^{N} (x(n))^2. \tag{9}$$

(2) Sample entropy: measuring the complexity of time series, the specific definition and calculation formula can be carried out according to the method proposed by Richman et al. [24].

(3) Spectral entropy: quantitative processing the smoothness of spectrum, which is positive correlation with feature show, if the relative power spectrum probability of $x(n)$ is P_k, the spectral entropy can be calculated as follows:

$$f_3 = -\sum_{K=0}^{N/2-1} P_k \ln(P_k). \tag{10}$$

(4) Mean value: describing the average value of amplitude change of acceleration signal in each area, which can be calculated according to the following formula:

$$f_4 = \frac{1}{N} \sum_{n=1}^{N} x(n). \tag{11}$$

(5) Median frequency: a measure used to describe the frequency change. First, calculating the power spectrum corresponding to the acceleration signal and then dividing the power spectrum probability into two parts with equal energy, the detail calculation process as references [25].

(6) Standard deviation: describing the variation amplitude of acceleration signal, solving according to the following formula:

$$f_6 = \sqrt{\frac{1}{N-1} \sum_{n=1}^{N} (x(n) - \overline{x})^2}. \tag{12}$$

(7) Skewness: a asymmetry measure of the vertical distribution near the mean, which is used to describe the asymmetry of acceleration signal when it changes and judge its change direction; the calculation is as follows:

$$f_7 = \frac{\sqrt{N(N-1)}}{N-2} \frac{1/N \sum_{n=1}^{N} (x(n) - \overline{x})^3}{\left(1/N \sum_{n=1}^{N} (x(n) - \overline{x})^2\right)^3}. \tag{13}$$

(8) Kurtosis: reflecting the kurtosis of the square distribution, which is used to describe the amplitude of

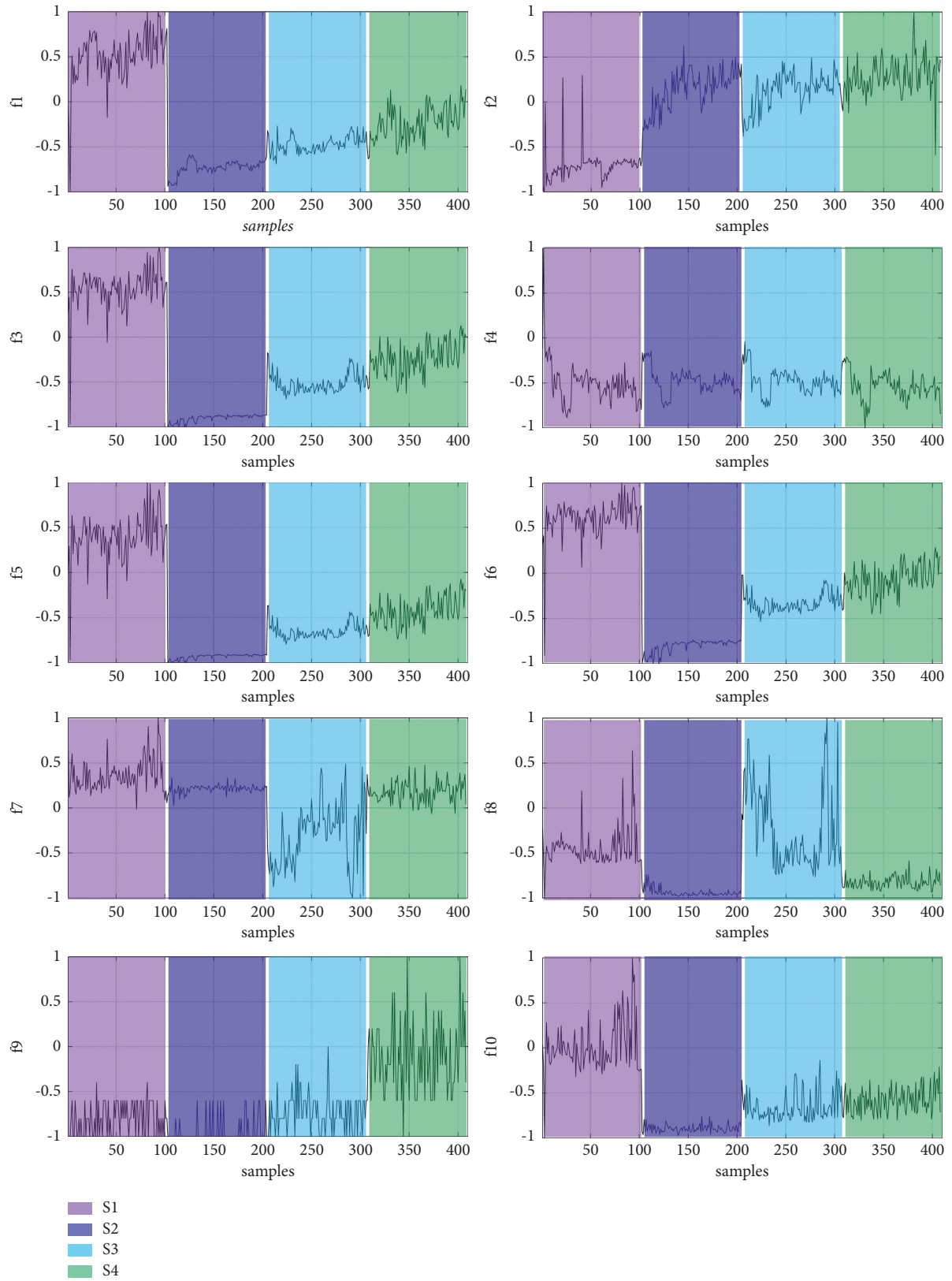

Figure 3: Features of samples.

acceleration signal change, the calculation is as follows:

$$f_8 = \frac{N-1}{(N-2)(N-3)}\left((N+1)\frac{1/N\sum_{n=1}^{N}(x(n)-\overline{x})^4}{\left(1/N\sum_{n=1}^{N}(x(n)-\overline{x})^2\right)^2} - 3(N-1)\right) + 3. \tag{14}$$

(9) Lempel-Ziv: a complex quantification method, reflecting the rate at which new patterns emerge in the time series and the detail calculation process as references [16].

(10) Crest factor: describing the peak sharpness of the signal, the calculation is as follows:

$$f_{10} = \frac{\max(x(n))}{\sqrt{1/N\sum_{n=1}^{N}(x(n))^2}}. \tag{15}$$

Acceleration signals in 102 pushing periods are collected in the laboratory environment; each period corresponds to the acceleration time series $x_i(n)$ of 4 pushing states, $i = 1, 2, 3, \ldots, 408$; the length of each time series is 2000, and finally, the eigenvalues corresponding to each acceleration time series are shown as f1–f10 in Figure 3. It can be seen from the figure that all the eigenvalues have a good recognition for the pushing states 1 and 2, but f4 is an exception. Between the pushing states 1 and 4, f4 nearly unchanged, and the boundaries are extremely blurred. Compared with f4, f9 has a good recognition for pushing state 4. When the features f1, f2, f3, and f10 are recognized in the pushing states 2–4, the recognition is low.

The other four eigenvalues, namely, f5–f8, have obvious boundaries for the four pushing states, especially f7 and f8. The consistency of all sample eigenvalues in the same state is very high, but the boundary of sample eigenvalues between different states is very obvious. Therefore, f5–f8 is the best choice among the above features used for pattern recognition of the pushing state. In order to verify the above assumption, first calculating the eigenvalues of all sample data and then arranging and combining all the eigenvalues, the total number of combinations is $\sum_{i=1}^{10} c_{10}^{i}$.Then, training each combination with SVM, calculating the k-fold cross-validation, and searching the optimal combination of each eigenvalue through the accuracy of the final 10-fold cross-validation, the final calculation results are obtained, as given in Table 1.

It can be seen from the results that the inspection accuracy of six combinations reached 99.8%, meanwhile f5–f8 exist in the six eigenvalue combinations. Considering the complexity of calculation and inspection accuracy, the eigenvalues f5–f8 are selected as the optimal combination, which verify the judgment results of the above eigenvalue selection.

3.3. SVM-Based Pushing State Recognition. Through the extraction and selection of the above feature values, finally, all the time series are converted into the training set (f5, f6, f7, f8) and the corresponding target state set (S1, S2, S3, S4)

Table 1: Combination result of the sample features.

f1	f2	f3	f4	f5	f6	f7	f8	f9	f10	CV
				√	√	√	√			**0.998**
		√	√	√	√	√	√	√		0.998
		√	√	√	√	√	√	√	√	0.998
			√	√	√	√	√			0.998
		√	√	√	√	√	√			0.998
				√	√	√	√	√	√	0.998
					√	√	√	√		0.997
					√	√	√	√	√	0.997
√	√	√	√	√	√	√	√	√	√	0.995
			√	√	√	√	√	√		0.995
			√	√	√	√	√	√	√	0.995
				√	√	√	√	√		0.995
					√	√	√			0.995
√	√	√	√	√	√	√	√			0.993
…	…	…	…	…	…	…	…	…	…	…

The values in bold means the best combination considering the cross validation results and the less features used in the algorithm.

of pushing state pattern recognition; it can be trained and predicated according to the training set and the target state set.

SVM is a machine learning method based on statistical theory proposed in the 1990s, which has a good application effect on pattern recognition problems with small samples and high dimensions. It can effectively avoid overfitting and has excellent nonlinear processing ability. By converting it into a convex quadratic programming problem, it can achieve the global optimum. If the given training samples are $(x_1, y_1), (x_2, y_2), \ldots, (x_n, y_n)$, in order to transform the input vector from a low-dimensional space x to a high-dimensional space z, first nonlinearly transform the input vector $z = H(x)$, solving weight vector w and offset B, and satisfy the following equation:

$$y_i\left(w^T \cdot z_i + b\right) \geq 1 \quad i = 1, 2, \ldots, l. \tag{16}$$

The unit vector of the weight vector is the normal direction of the interface. Therefore, the distance between the points close to the interface of the two categories is

$$d(w, b) = \min_{\{x|y=1\}} \frac{z^T \cdot w}{\|w\|} - \max_{\{x|y=-1\}} \frac{z^T \cdot w}{\|w\|}. \tag{17}$$

When the optimal boundary is reached, it should have met $w_o^T \cdot z + b_o = 0$, and the value of w_0 meets the requirements of the following formula:

$$d\left(w_o, b_o\right) = \frac{2}{\|w_o\|} - \frac{2}{w_o^T \cdot w_o}. \tag{18}$$

So far, the problem of solving the optimal interface is transformed into the following optimization problem:

$$\begin{aligned} &\min H(w) = \frac{1}{2}\left(w^T \cdot w\right) + V \cdot \sum_{i=1}^{l} a_i, \\ &\text{s.t } y_i\left(w^T \cdot z_i + B\right) \geq 1. \end{aligned} \tag{19}$$

Table 2: Commonly used kernel functions.

Name	Expression	Parameters
Linear kernel	$K(x_i, x_j) = x_i^T x_j$	None
Polynomial kernel	$K(x_i, x_j) = (x_i^T x_j)^d$	$d \geq 1$, polynomial degree
Gaussian kernel	$K(x_i, x_j) = \exp(-\|x_i - x_j\|^2/2\sigma^2)$	$\sigma > 0$, bandwidth
Laplace kernel	$K(x_i, x_j) = \exp(-\|x_i - x_j\|/\sigma)$	$\sigma > 0$
Sigmoid kernel	$K(x_i, x_j) = \tanh(\beta x_i^T x_j + \theta)$	$\beta > 0$ and $\theta < 0$

Table 3: Data samples after normalization.

f5	f6	f7	f8	State	f5	f6	f7	f8	State
0.025	0.321	0.648	−0.214	S1	0.302	0.563	0.339	−0.480	S1
0.293	0.417	0.121	−0.579	S1	0.499	0.694	0.302	−0.511	S1
−0.969	−0.911	0.197	−1.000	S1	0.148	0.447	0.422	−0.570	S1
0.248	0.498	0.428	−0.626	S1	0.583	0.751	0.341	−0.566	S1
0.308	0.538	0.358	−0.601	S1	0.411	0.663	0.447	−0.348	S1
...	...	...	...	...	...	...	...	...	...
−0.996	−0.992	0.142	−0.885	S2	−0.944	−0.834	0.202	−0.963	S2
−0.980	−0.937	0.175	−0.945	S2	−0.997	−0.992	0.249	−0.815	S2
−0.953	−0.864	0.246	−0.828	S2	−0.987	−0.955	0.095	−0.823	S2
−0.987	−0.960	0.176	−0.928	S2	−0.937	−0.815	0.231	−0.943	S2
−0.990	−0.970	0.335	−0.739	S2	−0.948	−0.840	0.158	−0.924	S2
...	...	...	...	...	...	...	...	...	...
−0.591	−0.270	−0.489	0.446	S3	−0.627	−0.294	−0.687	0.175	S3
−0.625	−0.301	−0.702	0.039	S3	−0.719	−0.415	−0.592	0.163	S3
−0.475	−0.127	−0.609	0.154	S3	−0.715	−0.409	−0.045	−0.537	S3
−0.656	−0.347	−0.875	0.770	S3	−0.675	−0.354	−0.272	−0.371	S3
−0.637	−0.322	−0.799	0.763	S3	−0.765	−0.486	−0.459	0.070	S3
...	...	...	...	...	...	...	...	...	...
−0.469	−0.109	0.400	−0.708	S4	−0.436	−0.067	0.178	−0.938	S4
−0.525	−0.173	0.250	−0.867	S4	−0.519	−0.158	0.228	−0.924	S4
−0.205	0.155	0.264	−0.804	S4	−0.464	−0.098	0.270	−0.838	S4
−0.124	0.236	0.046	−0.841	S4	−0.147	0.204	0.386	−0.796	S4
−0.440	−0.069	0.144	−0.809	S4	−0.074	0.287	0.092	−0.846	S4
...	...	...	...	...	...	...	...	...	...

Converting the objective function with the Lagrange multiplier algorithm,

$$L(w, b, \lambda) = \frac{1}{2}\left(w^T \cdot w\right) + V \cdot \sum_{i=1}^{l} a_l - \sum_{i=1}^{l} \lambda_i \left[y_i\left(w^T z_i + b\right) - 1\right],$$

$$f(z) = \operatorname{sgn}\left[\left(w^T \cdot z\right) + b\right] = \operatorname{sgn}\left[\sum_{i=1}^{l} \lambda_i \cdot y_i \cdot \left(z^T z_i\right)\right]$$

$$= \operatorname{sgn}\left[\sum_{\text{SupportVector}} \lambda_i \cdot y_i \cdot \left(z^T z_i\right) + b\right]. \tag{20}$$

In essence, SVM transforms samples into high-dimensional linear separable space through nonlinear transformation function H and constructs hyperplane to classify and recognize them. This nonlinear transformation function is also called kernel function, which satisfies the Mercer condition, $K(xi, yi) = H(xi)\, H(xj)$. Different kernel functions have different effects on SVM performance. The selection of kernel functions includes the selection of type and parameters. The commonly used kernel functions are given in Table 2.

Table 4: SVM detection result using different kernel functions.

Kernel function	k-fold	Test accuracy
Linear kernel	0.9938	0.9919
Polynomial kernel	0.9875	1.0000
RBF kernel	0.9939	1.0000
Sigmoid kernel	0.2250	0.2279

In addition to the above common kernel functions, we can also customize the kernel functions. If $K_1(x, x')$ and $K_2(x, x')$ are both kernel functions, we can customize the kernel functions through the following methods:

$$\begin{aligned}
K(x, x') &= c \cdot K_1(x, x') \\
K(x, x') &= f(x) \cdot K_1(x, x') \cdot f(x') \\
K(x, x') &= \exp\left[K_1(x, x')\right] \\
K(x, x') &= K_1(x, x') + K_2(x, x') \\
K(x, x') &= K_1(x, x') \cdot K_2(x, x') \\
K(x, x') &= K_1(\varphi(x), \varphi(x')) \\
K(x, x') &= x^T \cdot A \cdot x'.
\end{aligned} \tag{21}$$

In this section, the median frequency f5, standard deviation f6, skewness f7, and kurtosis f8 of the acceleration

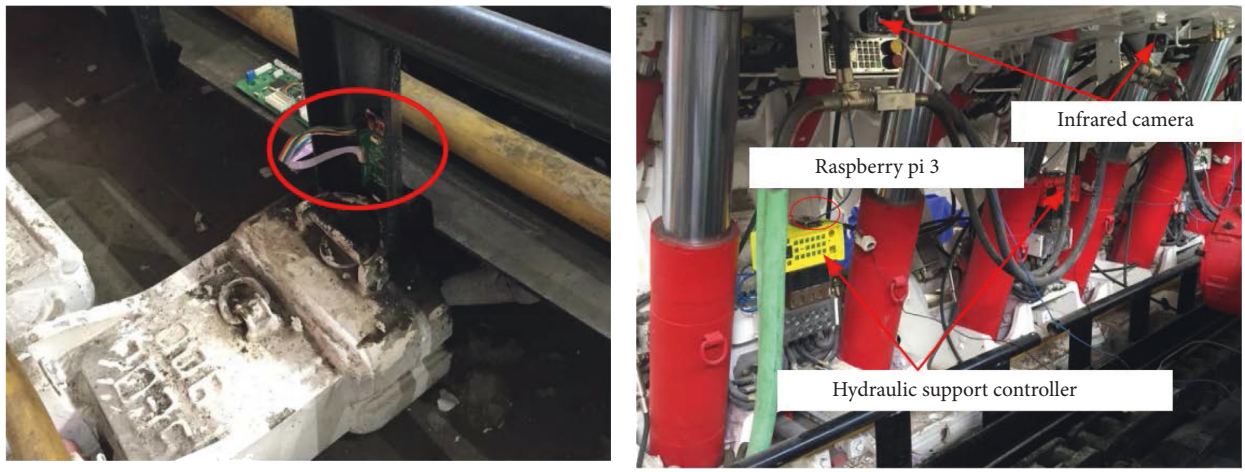

(a) (b)

Figure 4: IMU sensor installation position and experimental site. (a) IMU sensor installation position. (b) Experimental platform site.

signal are used as the input vectors of SVM, and the OVR method is used to realize the pushing state pattern recognition of MSR based on SVM. After the normalized processing of the acceleration signal collected on-site, the training sample set data obtained are given in Table 3.

Taking 60% of the sample data as the training set and the remaining 40% as the test set, the LibSVM library is used to realize the pushing state pattern recognition program in the MATLAB environment and calculating the k-fold cross test accuracy ($k = 10$) of the training set and the SVM classification results of the test set with different kernel functions. The results are given in Table 4.

It can be seen that RBF kernel function has better recognition accuracy when recognizing the pushing state in SVM, and the average recognition accuracy can reach 99.39%. Therefore, using RBF kernel function can achieve a better SVM classification effect and then realize the pushing state pattern recognition with high accuracy.

4. Experimental Research

4.1. Experimental Platform. Build the pose sensing experimental system of MSR through adding an IMU sensor to the original MSR sensing system. For the higher acquisition frequency and detection accuracy, the ADIS16448 IMU sensor is used for pushing pose sensing, as shown in Figure 4(a). In order to realize the pushing pose sensing, the whole experimental platform includes 4 MSRs, 1 shearer, 1 scraper conveyor, and other equipment. The experimental site is shown in Figure 4(b).

The MSR controller designed in this study is shown in Figure 5. The upper computer is installed with the monitoring software based on openPOWERLINK, which is an open-source industrial ethernet stack implementing the POWERLINK protocol for managing node and controlled node, designed to realize the remote operation of the controller, and the following action of MSR is controlled through POWERLINK. At the same time, the virtual monitoring system of MSR based on Unity3D is designed in C#.NET platform, which reproduces the pose of the real MSR in real time through the action of the virtual model of MSR with the pose data uploaded by Ethernet; the user interface is shown in Figure 5.

4.2. Experiment and Analysis. The pushing pose of MSR includes the attitude angle and displacement of the middle groove. The attitude angle of the middle groove can be calculated directly according to IMU, but the displacement needs more in-depth research. In order to verify the effectiveness of the pushing sensing method based on pushing state pattern recognition proposed in this study, the IMU sensor is installed on the middle groove of the scraper conveyor to obtain the inertia information in the moving process.

The denoising data samples of acceleration and angular velocity are shown in Figure 6. It can be seen from the figure that four state changes will occur in a cycle. When the state changes, the acceleration and angular velocity will change. According to the change characteristics of acceleration data, the pattern recognition of pushing state can be realized, and then, the acceleration data are processed in phases. Through the structural parameters of MSR, the theoretical sliding and support-moving speeds can be calculated. While, according to the measured displacement, the sliding and support-moving speeds can be calculated as 14.53 mm/s and 35.19 mm/s, respectively. Due to the influence of the current experimental environment and sensor noise, there is a certain error between the measured value and the theoretical value, and the error is given in Table 5.

Conduct the denoised IMU data with time interception, calculate the eigenvalues f5, f6, f7, and f8 corresponding to the IMU data in each time window, and identify the state in the current time window with the trained SVM model. Each state mode identified in a time window is shown in Figure 7 There is high accuracy in identifying the SVM state with eigenvalues f5, f6, f7, and f8, but there are also abnormalities in the case of large vibration. In Figure 7, the recognition

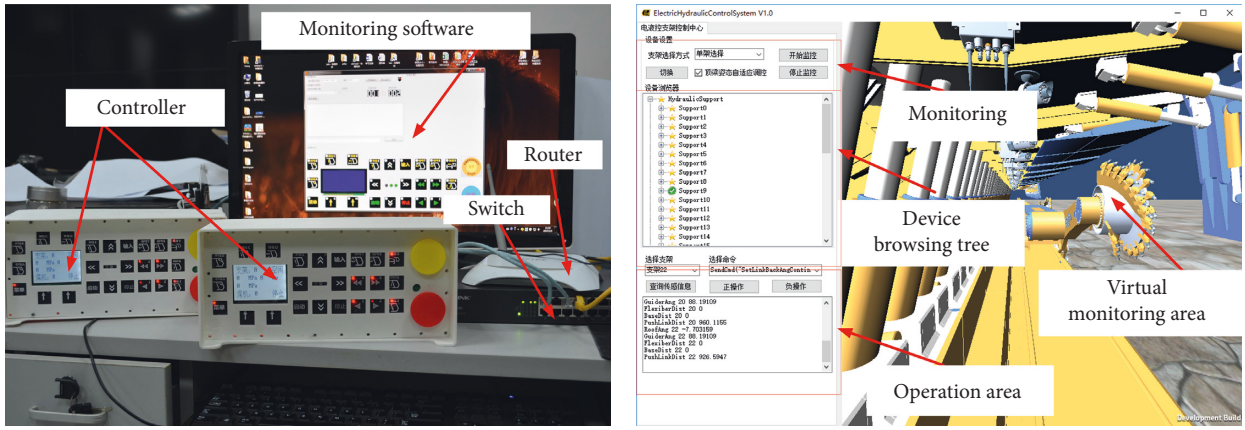

(a) (b)

Figure 5: Experimental platform for the AFM control system. (a) Autonomous follow-up controller. (b) Virtual monitoring system.

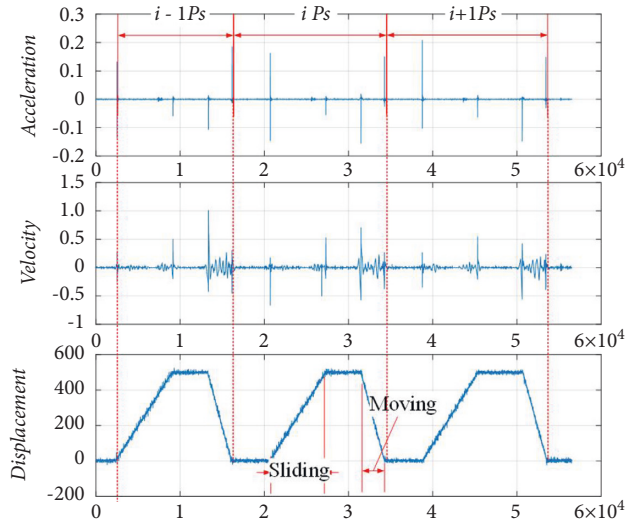

Figure 6: Data samples for pushing pose sensing.

Table 5: Pushing velocities.

Action	Ground truth (mm/s)	Measurement (mm/s)	Error (%)
Sliding	15.00	14.53	0.13
Support-moving	35.00	35.19	0.54

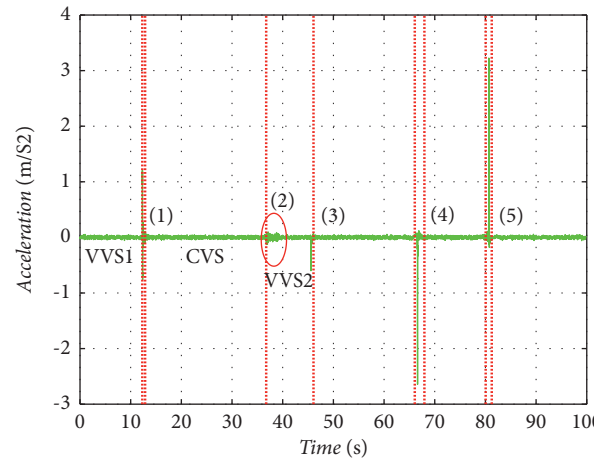

Segmental point
(1)Sliding start [2507, 2617];
(2)Vibration [7399, 7822];
(3)Sliding end [9141, 9261];
(4)Moving start [13285, 13448];
(5)Moving end [16054, 16292]
Sampling frequency: 200 Hz

Figure 7: Recognition result of the pushing state.

rates of the three states of sliding start, support-moving start, and support-moving end are accurate and the corresponding times are (12.53, 13.08), (66.41, 67.24), and (80.27, 81.46), respectively. However, there is a large vibration before the end of sliding, so the recognition rate in this area is low. In order to eliminate the influence of vibration on the pattern recognition of pushing state, it is clustered into the nearest state pattern in the time domain, and the vibration area in the figure is determined as the end of sliding.

According to the pattern recognition results of the pushing state, different IMU data phases are obtained, as shown in Figure 7; phase (1) is the sliding start phase, the sliding speed increases from 0 to the theoretical speed, corresponding to the first VVS phase (VVS1); phase (3) is the sliding end phase, which is the deceleration phase, corresponding to the second VVS phase (VVS2). Between VVS1 and VVS2 is the uniform speed phase, which is the first CVS phase (CVS). For VVS and CVS phase, Kalman filter estimation is performed according to their corresponding state space models, and the results are shown in Figures 8(a)–8(c).

In the VVS1 phase, if the integral method is directly adopted, a large cumulative error will occur in the acceleration phase of pushing jack. As shown in Figure 8(a), the final speed obtained by the integral method is more than 30 mm/s, while the theoretical value is only 15 mm/s. The value estimated by IFOA-KF is more accurate, and the final speed is maintained near the theoretical value. Similarly, for

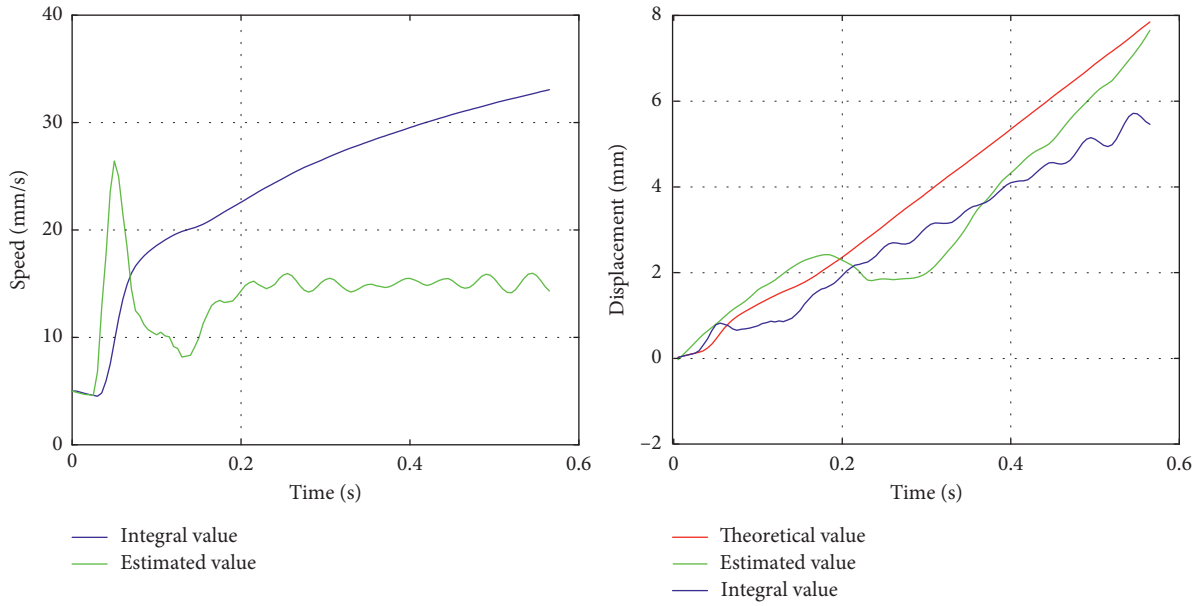

(a)

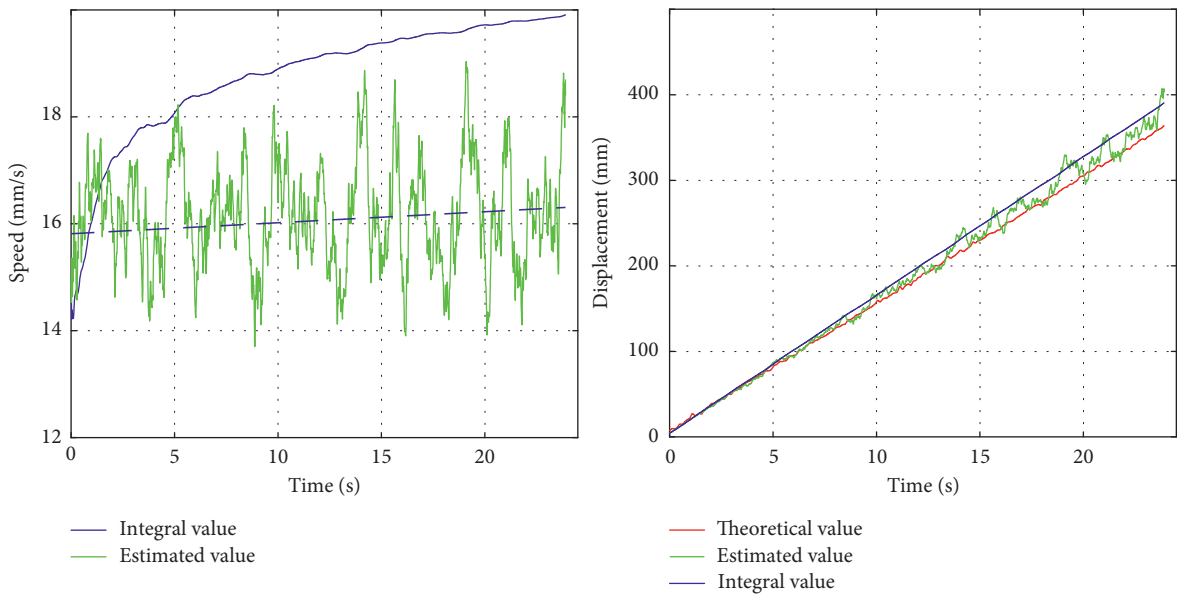

(b)

Figure 8: Continued.

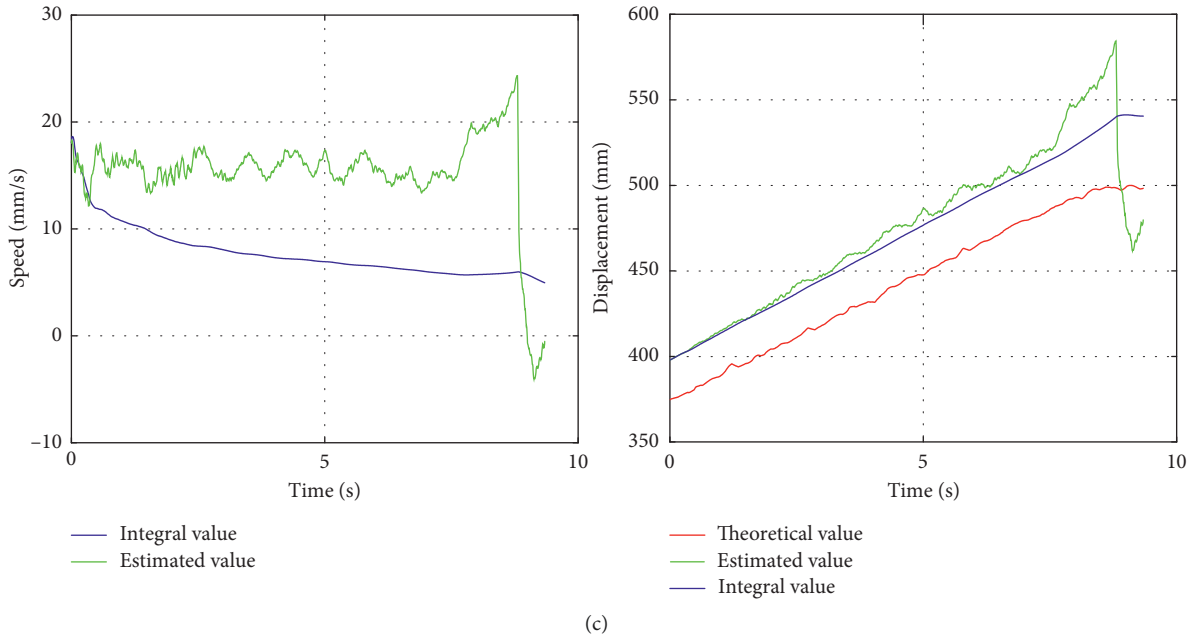

(c)

Figure 8: Segmental sensing result. (a) VVS1 segment. (b) CVS1 segment. (c) CVS2 segment.

Table 6: Error analysis result.

Phase	MSE	
	IFOA-KF method	Integration method
VVS1	0.349	0.581
CVS	5.830	12.442
VVS2	28.218	31.472

the estimation of displacement, the final result of IFOA-KF is closer to the theoretical value, and its mean square error MSE is 1.4615.

In the CVS1 phase, the initial displacement and velocity are determined by VVS1, and its initial condition is $[y_0, v_0, a_0]^T = [5.69, 15.02, 0]^T$. Due to the longtime of this period, the possibility of time cumulative error is greater. As shown in Figure 8(b), theoretically, this phase should move at a uniform speed, and the speed should be maintained at about 15 mm/s; however, the direct integration method produces a large error, resulting in a large displacement error in the final integration. In the VVS2 phase, the initial condition is the end condition of the CVS phase, that is, $[y_0, v_0, a_0]^T = [397.80, 18.01, 0]^T$. The results of integration and estimation are shown in Figure 8(c). The error of velocity and displacement estimated by IFOA-KF is much smaller than that obtained by the direct integration method, and the error analysis results are given in Table 6.

5. Conclusion

By analyzing the composition and characteristics of pushing pose of MSR and middle groove, a fusion evaluation model, which combines the pushing displacement-based least squares straightness and the pushing pose-based straightness of the middle groove, is established for realizing pushing pose alignment. To improve accuracy and reliability in the straightness evaluation process, a segmented sensing approach based on pushing state pattern recognition is proposed by selecting 4 difference features from typical IMU data features. The selected features are used for SVM training. The trained model can effectively recognize the pushing state pattern of MSR. To test and analyze the feasibility of proposed approach, a pose sensing experiment platform is built, and different motion stages of MSR are verified by experiments. Results show that estimation errors are significantly reduced compared with the traditional algorithm.

Data Availability

The data generated or analyzed during this study are included within the article and are available from the corresponding author upon request.

Conflicts of Interest

The authors declare that they have no conflicts of interest.

Acknowledgments

This work was supported by part of the National Natural Science Foundation of China (52004034), the Science and Technology Research Program of Chongqing Municipal Education Commission (KJQN202101413), Nature Science Research Key Project of Suzhou University (2017yzd14 and 2019yzd03), and the Natural Science Research Project in Universities of Anhui Province in China (KJ2021A1115).

References

[1] D. L. Wang, X. T. Zeng, G. F. Wang, and R. Li, "Stability of a face guard in a large mining height working face,"

International Journal of Simulation Modelling, vol. 20, no. 3, pp. 547–558, 2021.

[2] X. T. Zeng, G. Y. Meng, and J. H. Zhou, "Analysis on the pose and dynamic response of hydraulic support under dual impact loads," *International Journal of Simulation Modelling*, vol. 17, no. 1, pp. 69–80, 2018.

[3] Y. Zhang, H. Zhang, K. Gao, W. Xu, and Q. Zeng, "New method and experiment for detecting relative position and posture of the hydraulic support," *IEEE Access*, vol. 7, Article ID 181842, 2019.

[4] H. Tu, S. Tu, Y. Yuan, F. Wang, and Q. Bai, "Present situation of fully mechanized mining technology for steeply inclined coal seams in China," *Arabian Journal of Geosciences*, vol. 8, no. 7, pp. 4485–4494, 2015.

[5] A. Boutrid, M. C. Djouamaa, M. Chettibi, A. Bouhedja, and K. Talhi, "Design of a model powered support system in Kenadsa mine (Algeria)," *Journal of Mining Science*, vol. 52, no. 1, pp. 78–86, 2016.

[6] K. Gao, W. Xu, H. Zhang, Y. Zhang, Q. Zeng, and L. Sun, "Relative position and posture detection of hydraulic support based on particle swarm optimization," *IEEE Access*, vol. 8, Article ID 200789, 2020.

[7] X. Lu, Z. Wang, H. Yan, L. Si, and C. Tan, "Optimization design of pushing distance estimation of hydraulic support using the Kalman filter with the covariance improvement," *Advances in Mechanical Engineering*, vol. 11, no. 5, Article ID 168781401985072, 2019.

[8] X. Ge, J. Xie, X. Wang, Y. Liu, and H. Shi, "A virtual adjustment method and experimental study of the support attitude of hydraulic support groups in propulsion state," *Measurement*, vol. 158, Article ID 107743, 2020.

[9] S. Li, J. Xie, F. Ren, X. Zhang, X. Wang, and B. Wang, "Virtual straightening of scraper conveyor based on the position and attitude solution of industrial robot model," *International Journal of Coal Science & Technology*, vol. 8, no. 5, pp. 1149–1170, 2021.

[10] S. Li, J. Xie, X. Wang, F. Ren, X. Zhang, and Q. Bao, "Path planning of hydraulic support pushing mechanism based on extreme learning machine and descartes path planning," *Symmetry*, vol. 13, no. 1, p. 97, 2021.

[11] X. Wang, S. Li, and J. Xie, "Straightening method of scraper conveyor driven by robot kinematics and time series prediction," *Journal of China Coal Society*, vol. 46, no. 2, pp. 652–666, 2021.

[12] X. Yang, R. Wang, and H. Wang, "Pose measurement of detection robot IN hydraulic support based on motion process restoration method," *Journal of Taiyuan University of Technology*, vol. 51, no. 02, pp. 162–170, 2020.

[13] X. Zhang, D. Wang, and W. Yang, "Position detection method of hydraulic based on visual measurement," *Industrial and mining automation*, vol. 45, no. 03, pp. 56–60, 2019.

[14] H. Chen, H. Chen, Y. Xu, D. Zhang, Y. Ma, and J. Mao, "Research on attitude monitoring method of advanced hydraulic support based on multi-sensor fusion," *Measurement*, vol. 187, Article ID 110341, 2022.

[15] X. Yang, R. Wang, H. Wang, and Y. Yang, "A novel method for measuring pose of hydraulic supports relative to inspection robot using LiDAR," *Measurement*, vol. 154, Article ID 107452, 2020.

[16] M. Liang, X. Fang, S. Li, G. Wu, M. Ma, and Y. Zhang, "A fiber Bragg grating tilt sensor for posture monitoring of hydraulic supports in coal mine working face," *Measurement*, vol. 138, pp. 305–313, 2019.

[17] B. Wang, J. Xie, X. Wang, S. Liu, and Y. Liu, "A new method for measuring the attitude and straightness of hydraulic support groups based on point clouds," *Arabian Journal for Science and Engineering*, vol. 46, no. 12, Article ID 11739, 2021.

[18] S. Wang, Y. He, and S. Wang, "Study on the alignment method and experiment of scraper conveyor," *Journal of China Coal Society*, vol. 42, no. 11, pp. 3044–3050, 2017.

[19] Z. Meng, Q. Zeng, and L. Wan, "Pose adjusting simulation of hydraulic support based on mechanical-electrical-hydraulic coordination," *Tehnički Vjesnik*, vol. 25, no. 4, pp. 1110–1118, 2018.

[20] J. Xie, X. Wang, Z. Yang, and S. Hao, "Virtual monitoring method for hydraulic supports based on digital twin theory," *Mining Technology*, vol. 128, no. 2, pp. 77–87, 2019.

[21] J. Xie, X. Wang, Z. Yang, and S. Hao, "Attitude-aware method for hydraulic support groups in a virtual reality environment," *Proceedings of the Institution of Mechanical Engineers - Part C: Journal of Mechanical Engineering Science*, vol. 233, no. 14, pp. 4805–4818, 2019.

[22] J. Wang, Z. Wang, J. Xu, C. Tan, and L. Si, "Moving distance measurement for hydraulic support based on fruit fly optimization algorithm," *Optical Engineering*, vol. 56, no. 1, Article ID 013111, 2017.

[23] X. Lu, Z. Wang, C. Tan, H. Yan, L. Si, and D. Wei, "A portable support attitude sensing system for accurate attitude estimation of hydraulic support based on unscented kalman filter," *Sensors*, vol. 20, no. 19, p. 5459, 2020.

[24] J. Wen and Z. Lian, "The communication protocol design of electro-hydraulic control system for hydraulic supports at coal mine," *Web Information Systems and Mining*, vol. 6987, pp. 73–78, 2011.

[25] X. Zhang, P. Xia, Y. B. Cui, Y. Q. Liu, X. X. Liu, and Y. Y. Wang, "Software and hardware design of signal acquisition system about electro-hydraulic control system of hydraulic support," *Advanced Materials Research*, vol. 889-890, pp. 906–910, 2014.